DIRECT EXTRUSION FREEFORMING OF CERAMIC PASTES

Xiaopeng Chi, Hongyi Yang, Shoufeng Yang and Julian R.G. Evans
Department of Materials, Queen Mary, University of London,
Mile End Road, London, E1 4NS, UK
Reviewed, accepted September 14, 2006

Abstract

Microextrusion freeforming of ceramic lattices from high solids ceramic pastes provides multi-scale hierarchical void structures with the advantages of low shrinkage stress and high sintered density. Alumina lattices were directly fabricated using 80-500 μm diameter filaments. We report here on the implementation of design and fabrication of these scaffolds for band gap materials and micro fluidic devices.

Keywords: scaffolds, extrusion freeforming, meta materials.

Introduction

Solid freeform fabrication (SFF) is a class of advanced manufacturing technologies which generate accurate geometrical objects directly from a three-dimensional computer image without part-specific tooling or human intervention[1]. Many SFF technologies have been developed to date and they vary in terms of building speed, surface finish, dimensional accuracy and material properties[2-5]. A sub-class of methods is based programmable microextrusion of filaments onto a building platform and includes fused deposition modelling FDM[6], fused deposition of ceramics FDC[7], multiphase jet solidification[8-10] and robocasting[5]. Another direct write assembly[11] method uses pH-controlled gelling of ceramic colloids or polymers to build positive or negative scaffolds[12].

In these mouldless ceramic fabrication methods, the main difference is the method of state change. Robocasting uses temperature control on a copper substrate to transform each layer from pseudoplastic (61 vol. % powder) to dilatant (64 vol. %)[5, 13, 14] for which further deformation is prevented. To avoid this complex control of drying kinetics, colloidal inks have been developed for robocasting and are assembled under non-wetting oil to prevent drying during assembly[15, 16].

The method of state change used here is decrease of solvent content. The paste, composed of ceramic, polymer and solvent has high yield strength but is able to weld to the previous layer before solidifying by solvent evaporation. Sufficient polymer content (≈32vol.% based on wet paste) eliminates extrusion defects resulting from dilatancy often found in water-based systems. High ceramic content (minimum based on wet paste≈48vol.%) results in low sintering shrinkage. The different volume percent based on wet paste and on dry paste is shown in table 1. Low solvent content results in low drying shrinkage. The high yield strength of the paste minimises deformation during fabrication giving higher manufacturing precision.

Table 1. Different volume percent based on wet paste and on dry paste

	Volume percent Based on wet paste/vol.%	Volume percent Based on dry paste/vol.%
polymer	32	40
Ceramic powder	48	60
solvent	20	0

This method knits any conceivable two-dimensional extruded filament pattern layer by layer. The non-volatiles (ceramic + polymer) constitute typically 70-80 vol.% mixture of ceramic powder and polymer and 20-30 vol.% volatile solvent (usually propan-2-ol). The drying-induced shrinkage after assembly was minimized to reduce distortion of the lattice.

Experimental Details

Equipment

A press head driven by micro-stepper motors (50,000 steps/rev, supplied by ACP&D Ltd., Ashton-under-Lyne, UK) with a 64-1 reduction box driving 1mm pitch ball screws (Automation Ltd., Oldham, UK) was used to extrude the paste. Hypodermic syringes (HGB81320 1ml, Hamilton GB, Ltd., Carnforth, U.K.) were used as extrusion plunger, piston and nozzle. Although shortened hypodermic needles performed well in early experiments on filament diameters greater than 200 μm, smaller diameters blocked due to the long land length and orthogonal lead-in.

Superior extrusion dies were assembled from water-cut jet nozzles made from thin sapphire plates with smooth orifices, some models having a 45 degree lead-in cone. These were inserted into hypodermic needles. Very fine filaments (50 μm) can be extruded from these without blocking. A sensor (Flintec Ltd., Redditch, UK) monitored extrusion load and provided overpressure alarm.

The three axis table (Parker Hannifin Automation, Poole, Dorset, UK) comprises linear motor driven XY axes and stepper driven Z axis (Figure 1). Three axis motion, extruder drive, pressure and data recording were integrated by Labview software. An earlier version with a lead screw table locked at sharp reverse turns and was abandoned.

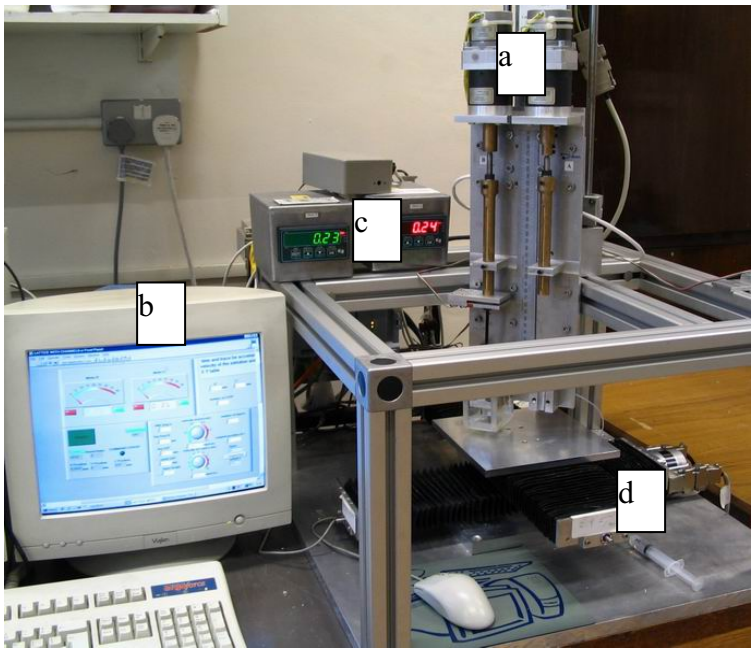

Figure 1. Extrusion freeforming apparatus, (a) twin extrusion presses on the Z axis, (b) computer control system, (c) load cell displays and alarms (d) linear motor XY table.

Paste preparation and extrusion

Alumina powder (HPA-0.5 Morgan Matroc Ltd, UK) was used for extrusion. Poly(vinyl butyral) (PVB), grade BN18 (Whacker Chemicals, UK) was used as the binder with additions of a grade of poly(ethylene glycol) (PEG) that is liquid at ambient temperature, (M_{Wt} = 600, VWR, UK). The PVB and the PEG were fully dissolved in propan-2-ol (GPR, VWR, UK) in proportion 75 wt.% PVB – 25 wt.% PEG. A powder blend with HA 75 wt. %-TCP 25 wt. %, [17], was added to provide a ceramic/polymer mixture with 60 vol.% of ceramic based on the dry mass and dispersed by ultrasonic probe (IKA U200S, IKA Labortechnik Staufen, Germany) for 15 minutes. The suspension was agitated on a roller table with zirconia media for 12 hours and dried to a paste for extrusion.

Results and Discussion

The final solids content determines the success of lattice fabrication. Each of five different pastes (30, 36, 39, 45 and 50 vol. % ceramic powder based on wet paste) were extruded to give lattices of different macro-porosity (50, 60, 70 and 80 %). In the fabrication process, the 'sinking' effect, whereby filaments sag between base-layer supports, results from high solvent contents and is shown in Figure 2. The 'curling' effect, in which the upper layer peels away from the base layer due to drying-induced stresses is shown in Figure 3a. The schematic diagram of the 'curling' effect is shown in Figure 3b. The angle of deformation, θ, can be obtained by the formula below:

$$\tan\theta = \frac{H}{L} \quad (1)$$

where, H is the drying deformation height; L is the drying deformation length along the filaments.

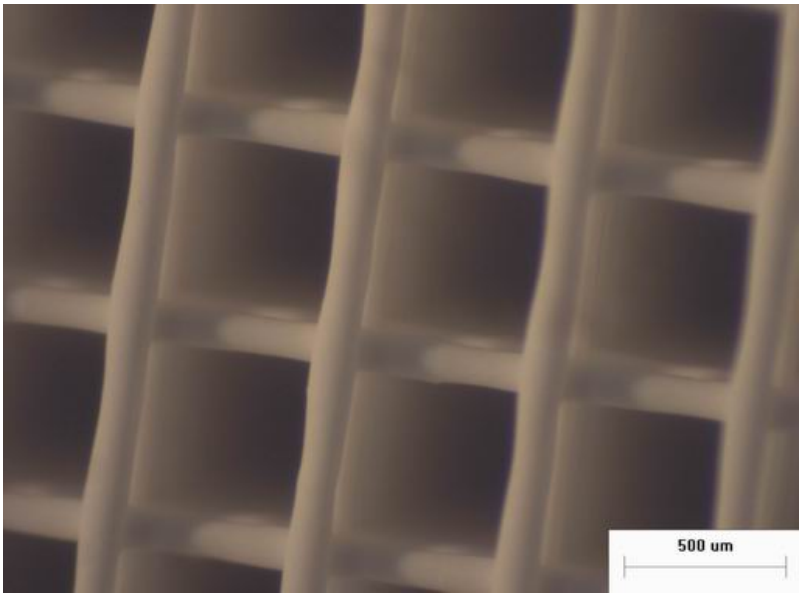

Figure 2. Filament 'sinking' effect resulting from high solvent content in an unsintered alumina lattice with 39 vol.% ceramic powder in the wet paste. The distance between filaments is 630μm.

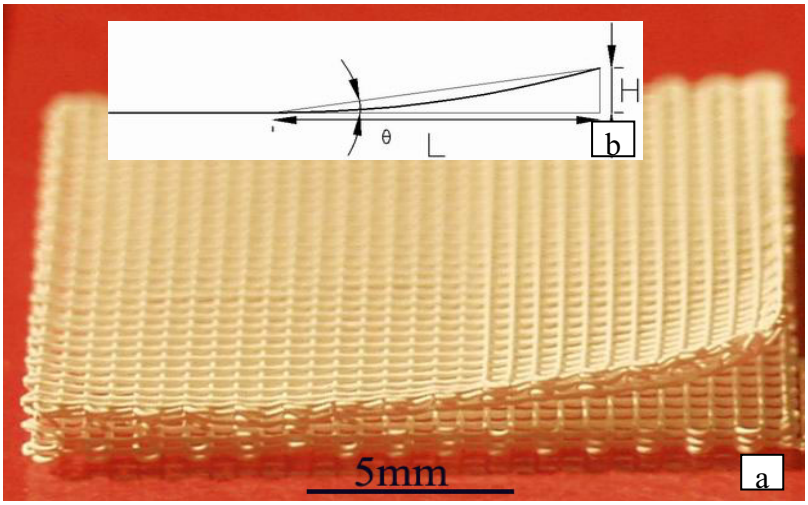

Figure 3. Drying defect in a 14 layer alumina lattice fabricated by the 39 vol.% ceramic powder in the wet alumina paste. The distance between filaments is 630μm.

Two factors influence the 'sinking' effect: the yield stress of the paste which is mainly influenced by solids fraction and the distance between filaments (span). Using the same paste, the span was systematically decreased which in turn decreases the macroporosity of the lattice[18,

[19]. Figure 4 shows that the largest detectable sinking distance decreases as the span decreases, i.e. as the lattice becomes less porous. Using a lattice with fixed span and hence fixed lattice porosity and systematically varying the solvent content with fixed ceramic-polymer ratio, the sinking distance decreases as the non-volatile fraction increases.

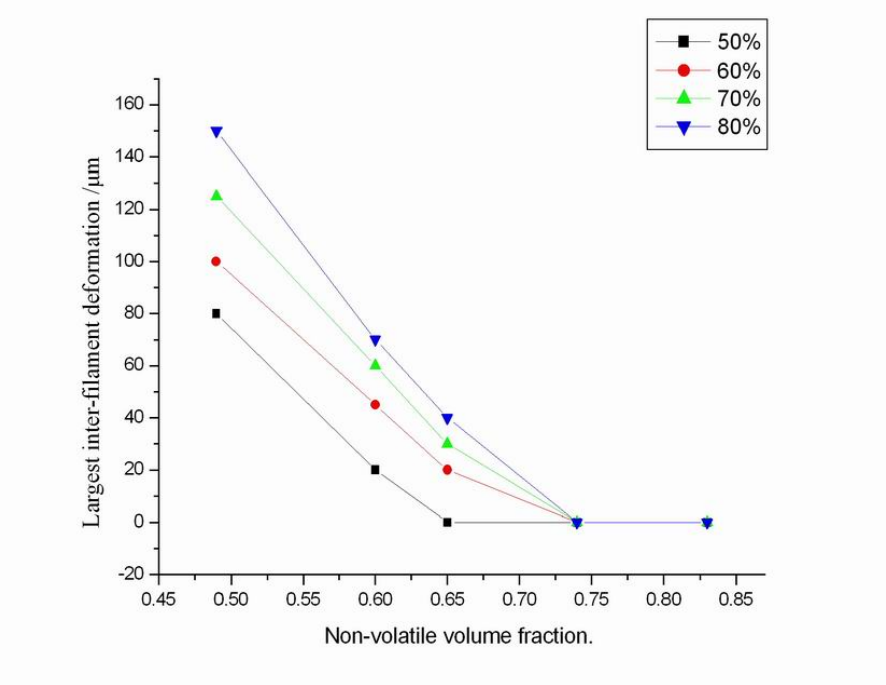

Figure 4. Sinking deformation as a function of the non-volatile fraction of the paste for different lattice spans; the largest observed inter-filament deformation was recorded. Note that a high lattice macroporosity (as given in the key) corresponds to a high span.

The curling effect is caused by the drying shrinkage stresses during fabrication. If the paste becomes a fully dense binary of ceramic and polymer after drying, the volume shrinkage is equal to the volume fraction of solvent. The linear shrinkage is 10% for 27 vol.% solvent. Four factors influence the extent of curling and delamination: (i) the powder fraction in the dried ink controls the elastic modulus of the 0-3 composite such that modulus typically increases steeply as the powder fraction exceeds 50 vol.%, (ii) the rate of volatilisation of solvent influences the differential shrinkage between layers; in the worst case scenario the base layer has fully dried so that its shrinkage is complete when the next layer begins to dry, (iii) the span between filaments determines the number of welds per unit area and hence overall laminate strength, (iv) as the span decreases and the lattice becomes more densely packed, the vapour transport within the structure decreases and drying rate slows down, in turn reducing drying deformation.

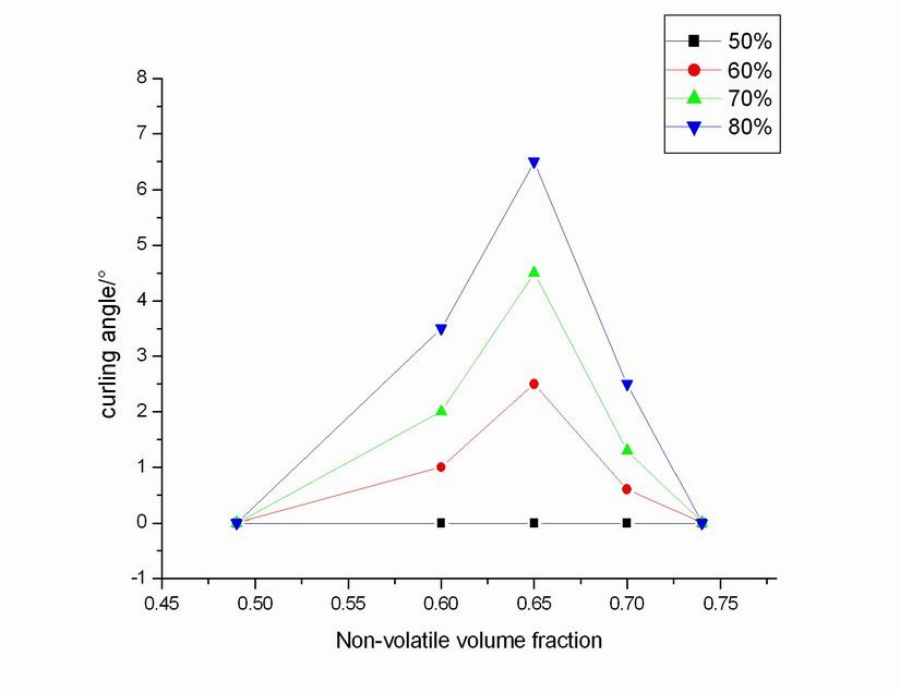

Figure 5. Deformation angle as a function of non-volatile fraction of the paste for different lattice spans.

From Figure 5, when the non-volatile content was less than 49 vol.%, the rendered layers remain wet while new layers are deposited. The increased weld strength between filaments counteracts delamination. Since the first layer is strongly adherent to the substrate, deformation did not occur whatever the lattice span. When the non-volatile content were between 49 and 65 vol.%, the weld strength decreased as the solvent content increased and could not counteract the shrinkage of filaments. Although the overall shrinkage decreased, the drying time was reduced. In this regime, drying deformation increased with increasing non-volatile content**.** When the non-volatile content was between 65 and 74 vol.%, the overall shrinkage of filaments decreased and drying deformation decreased with increasing non-volatile content. When the non-volatile content was more than 74 vol. %, the solvent was correspondingly low and so the linear shrinkage was low. The effect of lattice macroporosity is very pronounced. At high porosity, the number of welds per unit area is low and delamination is facilitated. Furthermore, the more open structure allows faster drying of rendered layers.

When the non-volatile content was greater than 74 vol. %, all these defect phenomena were absent as evidenced by the regular structures shown in Figures 6 and 8.

Theoretically, the span of the lattice can be made in any size by increasing the non-volatile volume fraction. In practice, the spans between filaments cannot be increased without limit[16, 18]. If the solvent content was less that 16 vol.%, the paste was too dry to weld to the base layer. The nozzle was easily blocked and the layers did not join. An ideal lattice was attained when the solvent content was approximately 26 vol. %.

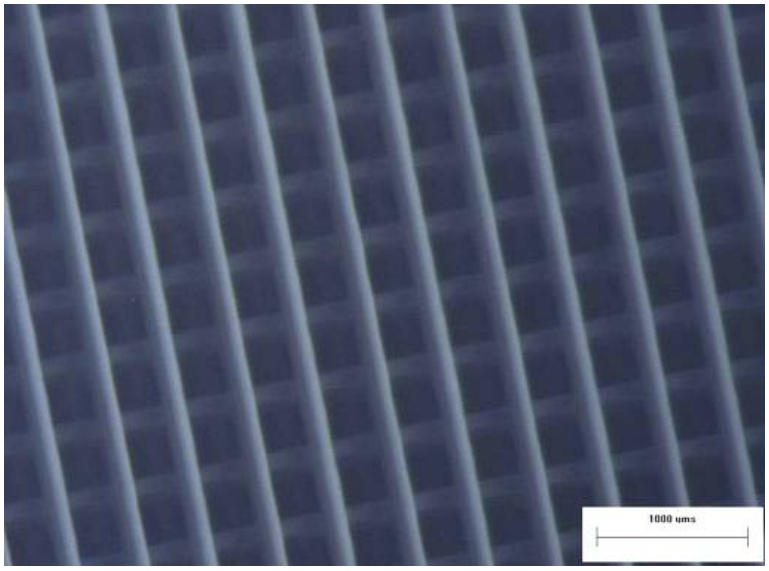

Figure 6. Unsintered alumina lattice with 26 vol. % solvent and inter-filament distance 630 µm showing no sagging or drying deformation.

The extrusion distance is the gap between the die exit and the previous layer. If the gap is too large, the filaments are difficult to control and may drag across the substrate. If the distance is set too small, the nozzle smears the paste and damages the filaments. The appropriate distance depends on the nozzle diameter and the viscosity of the paste. For the 150µm diameter nozzle, the best distance was 0.2 mm. The nozzle is raised on the Z axis before a new layer is started. Theoretically, the filament extrusion velocity V_r and the velocity of the XY table V_{XY} are compliant with:

$$V_{xy} = \left(\frac{R}{r}\right)^2 V_R \qquad (2)$$

where R and r are the diameter of the plunger and the nozzle respectively.

If $V_r < V_{XY}$, the filament was stretched and if $V_r > V_{XY}$ it formed curves. In practise, the viscous nature of the paste also delayed the response of the stress to the strain[19] so that filament extrusion speed V_r did not respond quickly to changes in the speed of the XY table V_{XY}. So many data around the ratio $\left(\frac{R}{r}\right)^2$ were tested to find out the optimal V_r and V_{XY}. To increase fabrication speed, rapid XY table movement V_{XY} and extrusion velocity V_r were needed, but this places high loads on the microextrusion press. So in this experiment, the speed of the XY

table V_{XY} was 6.735 mm/s and the speed of the filament extruded V_r was 0.00825 mm/s.

The alumina lattices were sintered at 1540°C for 1 hr after slow heating to 400°C at a rate of 2°C/min with 1 hour dwell so that the polymer in the samples could be removed slowly and evenly. The microstructure, observed by SEM and shown in Figure 8 is of near full density, with isolated residual porosity and average grain size in the region 3-4 μm.

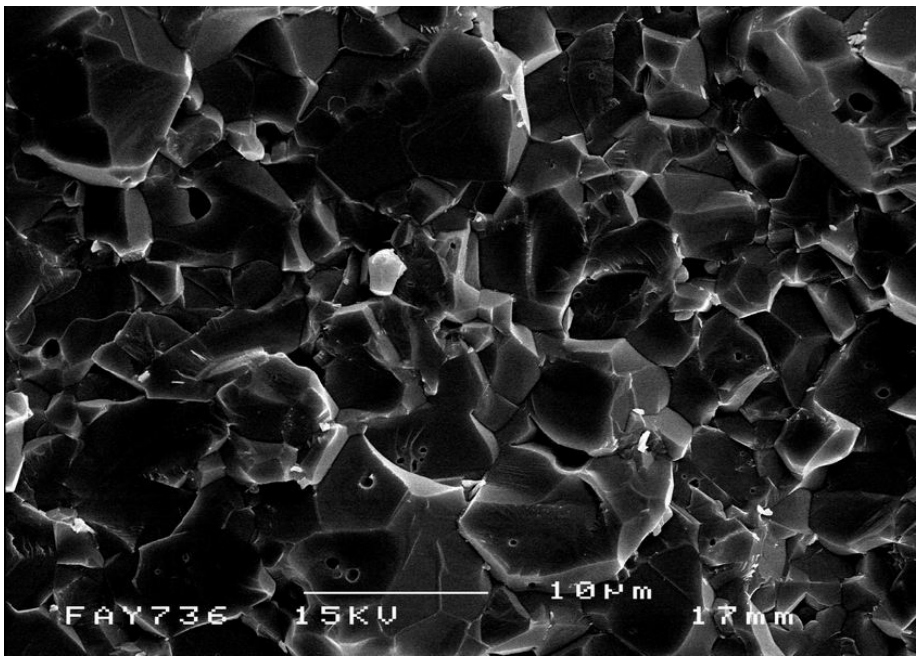

Figure 7. Microstructure of alumina filament sintered at 1540°C at 5°C/min with 1 hour dwell after heating to 400°C at 2°C/min.

Lattice design and fabrication

It is well known that periodic dielectric structures can block propagation of electromagnetic waves. One such structure is the 'woodpile' [20-22]. In this approach, woodpiles with different distances between filaments can be made by alumina filaments. Such 'woodpiles' with 630 μm between filaments are shown in Figure 8 and their dimensions in Table 2.

Table2. The dimensions of 20 layer alumina lattices with 74 vol.% non-volatile content.

	Length /mm	Width /mm	Height /mm	Filament Diameter /mm	Gap /mm	Shrinkage /%
Before sintering	19.68	19.68	2.90	0.15	0.63	20.2
After sintering	15.70	15.70	2.30	0.12	0.50	

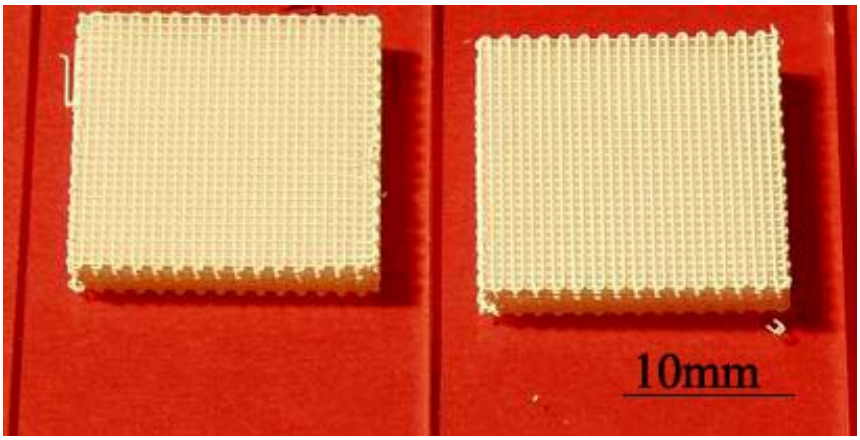

Figure 8. Unsintered alumina lattices comprising 20 layers prepared from a paste with 26 vol.% solvent, having an inter-filament distance of 630 μm.

When defects are made periodically in an electromagnetic band gap (EBG) structure, defect mode resonance can be created[23, 24]. So a lattice with square lacuna was designed and fabricated. The amplified square area of the lattice was drawn by Solidwork software as shown in Figure 9a. It was obvious that the width of the square was limited by the distance between filaments. However the distance between filaments cannot be made too big or filaments will sink. The sample with the square lacuna periodic structure was fabricated by extrusion freeforming and is shown in Figure 9b. The size of the samples and the shrinkage rate is given in Table 3.

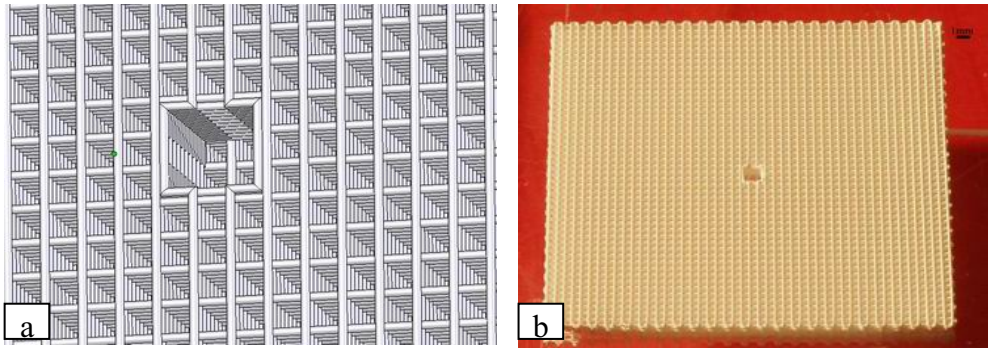

Figure 9. (a) Magnified square lacuna area of the lattice; (b) Micro-extruded alumina lattice with square lacuna.

Table3. Dimensions of lattice with square lacuna

	Length /mm	Width/ mm	Height /mm	Filament Diameter/mm	Gap/ mm	Lacuna size/mm	Shrinkage /%
Before sintered	30.64	30.64	2.90	0.15	0.48	1.59x1.59	20.7%
After sintered	24.62	24.62	2.30	0.12	0.38	1.26x1.26	

As applications for microfluidic reactors broaden, materials with higher temperature capability and chemical resistance are sought to fabricate the microfluidic reactor[25]. Ceramic microchannel devices have been fabricated by a prototyping process chain combining stereolithography and low-pressure injection molding[26], and by lamination[27]. An alumina microfluidic reactor was fabricated by extrusion freeforming in this work. The reactor was made up of five parts (shown in Figure 11a). The upper and lower covers were separately made up each of two layers assembled from alumina filaments attached each other tightly. The flow channels were made up of four layers assembled by alumina filaments with two large channels (2.55mm) to facilitate gas flow and 20 smaller channels (0.45mm) for the gas to disperse well. The mixing chamber was made up of four layers assembled by alumina filaments with 20 small channels (0.45mm) for gas mixing. The outflow was made up of four layers assembled by alumina filaments with one large channel (0.9mm) for the gas to exit. A schematic diagram of the two gas flows is shown in Figure 11b. The overall size of the reactor was 15.48 x 10.68 x 1.92mm after sintering and the small channel for the gas mixing was 0.36mm after sintering. An alumina microfluidic reactor without the lower cover is shown in Figure 12.

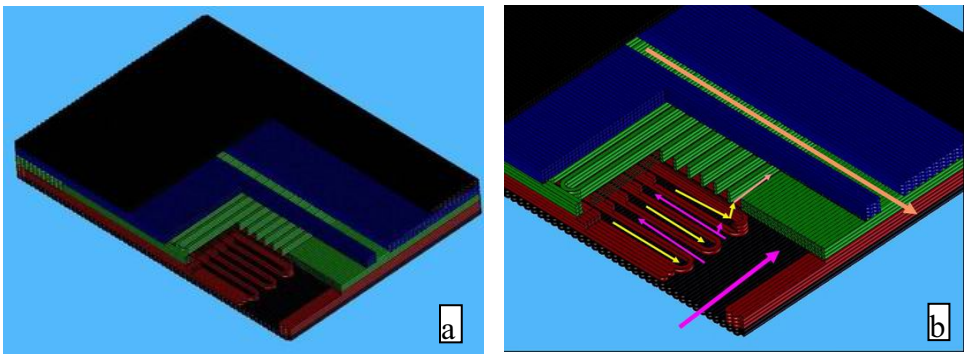

Figure 11 a) cutaway view of the alumina microfluidic reactor; b) schematic diagram of the two types of gas through the reactor.

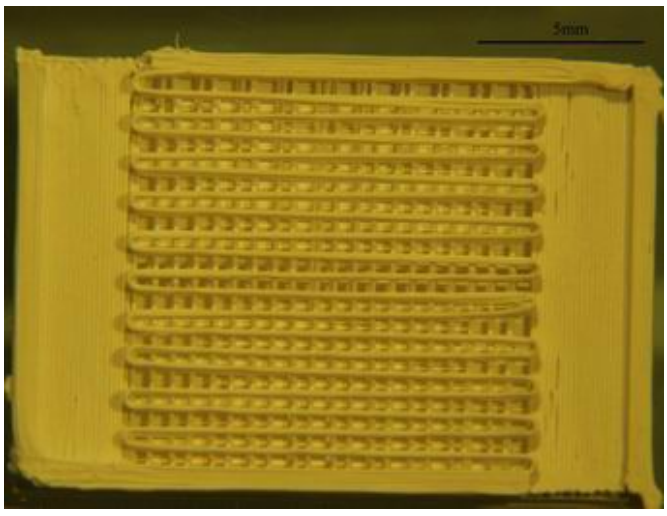

Figure 12. The alumina microfluidic reactor without the lower cover

Conclusions

It has been demonstrated that regular ceramic lattices can be fabricated by extrusion freeforming by adjustment of paste composition. Conditions for avoiding the characteristic defects of the process such as filament sagging between previous layers and drying deformation were obtained by controlling the solid loading of the paste, the extrusion rate, the X, Y table velocity, the filament diameter. Upon sintering, the alumina lattices have sintered densities greater than 95% and sintering shrinkage 20%. The procedure is ideally suited to prototyping of hard tissue scaffolds, electromagnetic bandgap structures and microreactors.

Acknowledgement

The authors are grateful to the Engineering and Physical Sciences Research Council (EPSRC) for supporting this work under grant number GR/S57068.

References

1. D.T. Pham, and R. S. Gault, , A Comparison of Rapid Prototyping Technologies, Int. J. Mach. Tool Manu., 1998, 38, 1257-1287.
2. M.K. Agarwala, et al, FDC, Rapid Fabrication of Structural Components, American Ceramic Society Bulletin, 1996, 75, 11, 60-65.
3. E.A. Griffin, et al, Rapid Prototyping of Functional Ceramic Composites, American Ceramic Society Bulletin, 1996, 75, 7, 65-68.
4. M.L. Griffith and J.W. Halloran, Freeform Fabrication of Ceramics via Stereolithography, J. Am. Ceram. Soc., 1996, 79, 10, 2601-08.
5. J. Cesarano III and A. Thomas, Recent Developments in Freeform Fabrication of Dense Ceramics from Slurry Deposition, Proceedings Solid Freeform Fabrication Symposium, University of Texas at Austin, 1997.
6. S.S.Crump, Proc. 2nd Int. Conf. on 'Rapid prototyping', Dayton, OH, University of Dayton, 1991, 354-357.
7. M. Allahverdi, A. Hall, R. Brennan, M. E. Ebrahimi, N. M. Hash and A. Safari, An Overview of Rapidly Prototyped Piezoelectric Actuators and Grain-Oriented Ceramics, J. electroceram., 2002, 8, 129-137.
8. M. Greul, T. Pintant and M. Greulich, Rapid Prototyping of Functional Metallic Parts, Comput. Ind., 1995, 28, 23-28.
9. M. Greul, R. Lenk, Near-Net-Shape Ceramic and Composite Parts by Multyphase Jet Solidification (MJS), Ind. Ceram., 2000,20,115-117.
10. M. Geiger, W. Steger, M. Greul and M. Sindel, Fast, Functional Prototypes via Multiphase Jet Solidification, EARP News-letter, 1994, (3).
11. S.L. Morissette, J.A. Lewis, J. Cesarano, D. Dimos, and T. Baer, Solid Freeform Fabrication of Aqueous Alumina-Poly(vinyl alcohol) Gelcasting Suspensions, J. Am. Ceram. Soc., 2000, 83 [10], 2409-16.
12. G. Gratson, M. Xu, and J.A. Lewis, Direct Writing of Three Dimensional Webs, Nature,

2004, 428-386.
13. J. Cesarano III, P. Calvert, Freeforming Objects with Low-Binder Slurry, US Patent 6,027,326.
14. J. Cesarano III, Solid Freeform and Additive Fabrication, Mater. Res. Soc. Symp. Proc., 1998, 542, 133-139.
15. E.S. James, J. Cesarano III, and J.A. Lewis, Colloidal Inks for Directed Assembly of 3-D Periodic Structures, American Chemical Society, 2002, 18, 5429-5437.
16. M. Sarah, W. Willie, J.A. Lewis, Concentrated Hydroxyapatite Inks for Direct-write Assembly of 3-D Periodic Scaffolds, Biomaterials, 2005, 26 632–5639.
17. H. Yang, S. Yang, X. Chi, J.R.G. Evans, Fine Ceramic Lattices Prepared by Extrusion Freeforming, J. Biomedical Materials Research, in printing.
18. E.S. James, J. Cesarano III, and J. A. Lewis, Colloidal Inks for Directed Assembly of 3-D Periodic Structures, American Chemical Society, 2002, 18, 5429-5437.
19. F.N. Cogswell, Polymer Melt Rheoogy, A Guide for Industrial Practice, John wiley and sons, New York and Toronto. 1981, p17.
20. E. Ozbay, A. Abeyta, G. Tuttle, M. Tringides, R. Biswas, C. T. Chan, C. M. Soukoulis, and K. M. Ho, Measurement of a Three-Dimensional Photonic Band Gap in a Crystal Structure Made of Dielectric Rods, Phys. Rev. B, 1994, 50 [3] 1945–48.
21. E. Ozbay, E. Michel, G. Tuttle, R. Biswas, M. Sigalis, and K. M. Ho, Micromachined Millimeter-Wave Photonic Band-Gap Crystals, Appl. Phys. Lett., 1994, 64, [16] 2059–61.
22. S. Y. Lin, J. G. Fleming, D. L. Hetherington, B. K. Smith, R. Biswas, K. M. Ho, M. M. Sigalis, W. Zubrzycki, and S. R. Kurtz, A Three Dimensional Photonic Crystal Operating at Infrared Wavelengths, Nature (London), 1998, 394, 251–53.
23. C.J. Reilly, W.J. Chappell, J.W. Halloran and L.P.B. Katehi, High-Frequency Electromagnetic Bandgap Structures via Indirect Solid Freeform Fabrication, J. Am. Ceram. Soc., 2004, 87 [8], 1446-1453.
24. E. Yablonovitch, T. J. Gmitter, R. D. Meade, A. M. Rappe, K. D. Brommer, and J. D. Joannopoulous, Donor and Acceptor Modes in Photonic Band Structure, Phys. Rev. Lett., 1991, 67, 3380.
25. P.M. Martin, D.W. Matson, W.D. Bennett, D.C. Stewart and C.C. Bonham, Laminated Ceramic Microfluidic Components for Microreactor Applications, in Proc. of the 4th Int. conf. on Microreaction Technology, IMRET 4, March 5-9, 2000, Atlanta, USA, 410.
26. R. Knitter, W. Bauer, et al., Manufacturing of Ceramic Microcomponents by a Rapid Prototyping Process Chain, Adv. Eng. Mater., 2001, 3[1-2] 49-54.